PHYSICAL REVIEW LETTERS **123,** 184501 (2019)

# Hydrodynamic *X* Waves

James N. Steer,[1] Alistair G. L. Borthwick,[1] Miguel Onorato,[2] Amin Chabchoub,[3] and Ton S. van den Bremer[4]
[1]*School of Engineering, University of Edinburgh, Edinburgh EH9 3FB, United Kingdom*
[2]*Dipartimento di Fisica, Università di Torino and INFN, Sezione di Torino, Via Pietro Giuria 1, 10125 Torino, Italy*
[3]*Centre for Wind, Waves and Water, School of Civil Engineering, The University of Sydney, Sydney, NSW 2006, Australia*
[4]*Department of Engineering Science, University of Oxford, Oxford OX1 3PJ, United Kingdom*

(Received 5 February 2019; published 29 October 2019)

Stationary wave groups exist in a range of nonlinear dispersive media, including optics, Bose-Einstein condensates, plasma, and hydrodynamics. We report experimental observations of nonlinear surface gravity *X* waves, i.e., *X*-shaped wave envelopes that propagate over long distances with constant form. These can be described by the $2D+1$ nonlinear Schrödinger equation, which predicts a balance between dispersion and diffraction when the envelope (the arms of the *X*) travel at $\pm\arctan(1/\sqrt{2}) \approx \pm 35.26°$ to the carrier wave. Our findings may help improve understanding the lifetime of extremes in directional seas and motivate further studies in other nonlinear dispersive media.

DOI: 10.1103/PhysRevLett.123.184501

Stationary or nondispersive wave groups can occur in a range of nonlinear dispersive media, including in optics [1–3], Bose-Einstein condensates [4], plasma [5], and hydrodynamics. In optics, families of linear localized wave (LW) solutions to the free-space scalar wave equation have been found [6–8]. One such family is the so-called "*X* wave" characterized by an *X*-shaped packet structure with a sharp, high amplitude centroid. Linear *X* waves have been observed and confirmed to be nondispersive in optical fibers [9]. Optical LWs play a role in free space communications [10], optical lithography [11], and optical rogue waves [12].

When the scales of group velocity dispersion (GVD) and nonlinear amplitude effects are comparable, nonlinearity must be considered. Whereas GVD can be described using a dispersion relationship, amplitude-dependent nonlinear effects are typically modeled through the universal nonlinear Schrödinger equation (NLSE) [13], which applies in nonlinear dispersive media [14,15], and can be extended to two spatial dimensions. Indeed, in optics, "light bullet" nonlinear *X* waves have been predicted and created experimentally [1,2], and extreme LW events or "rogue waves" have been detected in optical telecommunication fibers [16]. Because of the dispersive and nonlinear character of water waves, an analogy between water waves, optics, Bose-Einstein condensates, and plasma can be naturally drawn [3,17–20].

Both the coupled NLSE (CNLSE) (whereby two nonlinear systems interact) and the $2D+1$ NLSE (whereby one system exists with a crossing angle $\theta$ between the carrier and envelope) can describe the evolution of crossing, weakly nonlinear wave systems. Using the $2D+1$ NLSE, a critical crossing angle of $\theta_c = \pm\arctan 1/\sqrt{2}$ can be derived, beyond which linear focusing becomes defocusing, and the system achieves stability to sideband perturbations [21]. In the CNLSE, a similar stabilization of the coupled system is observed at the same critical angle [22]. For hydrodynamics and at low interaction angles, numerical simulations and experimentation have confirmed these predictions, observing an increase in the kurtosis of crossing seas up to approximately ±25° that reduces rapidly as the angle is increased towards $\theta_c$ [23]. These results have been confirmed using phase-resolving numerical simulations for realistic broadbanded crossing sea states, showing that the maximum kurtosis is small at the critical angle, with the minimum occurring at slightly larger angles [24].

In hydrodynamics, wave groups propagating at the critical crossing angle predicted by the $2D+1$ NLSE occur naturally at the fringes of the Kelvin ship wake [25]. Furthermore, an isolated spectral energy peak tends to spread outwards at this angle [26]. Through the elimination of dispersion at the critical angle, it may be possible to extend dramatically the lifetime of groups containing extreme events. Indeed, previous numerical studies on the three-dimensional evolution of long-crested waves perturbed using random phases have shown natural formation of slanted coherent structures [27] that interact to produce long-lived rogue waves [28,29].

In this experimental study, we create for the first time a nondispersive hydrodynamic *X* wave. We measure the spatiotemporal free surface elevation of the *X* wave, and compare it with numerical solutions of the $2D+1$ NLSE.

*Theoretical background.*—We consider the $2D+1$ NLSE for deep-water surface gravity waves [30]:

$$i\left(\frac{\partial A}{\partial t} + c_g \frac{\partial A}{\partial x}\right) - \alpha \frac{\partial^2 A}{\partial x^2} + 2\alpha \frac{\partial^2 A}{\partial y^2} - \beta |A|^2 A = 0, \quad (1)$$

where $x$ and $y$ are the horizontal coordinates, $t$ is time, and $A(x, y, t)$ the envelope of a carrier wave of frequency $\omega_0$ and wave number $\boldsymbol{k}_0 = (k_0, 0)$ propagating in the $x$ direction. The coefficients of the 2D-NLSE are

$$c_g = \frac{\partial \omega}{\partial k_x}\bigg|_{\boldsymbol{k}=\boldsymbol{k}_0} = \frac{\omega_0}{2k_0}, \tag{2a}$$

$$\alpha = \frac{1}{2}\frac{\partial^2 \omega}{\partial k_x^2}\bigg|_{\boldsymbol{k}=\boldsymbol{k}_0} = \frac{\omega_0}{8k_0^2}, \tag{2b}$$

$$\beta = \frac{\omega_0 k_0^2}{2}. \tag{2c}$$

While the second derivative in $x$ is responsible for envelope dispersion, the second derivative in $y$ implies diffraction. The leading-order identity $\partial A/\partial t \simeq -c_g \partial A/\partial x$ can be used to transform the $2D + 1$ NLSE to a form suitable for laboratory experiments [31,32],

$$i\left(\frac{\partial A}{\partial x} + \frac{1}{c_g}\frac{\partial A}{\partial t}\right) - \frac{\alpha}{c_g^3}\frac{\partial^2 A}{\partial t^2} + \frac{2\alpha}{c_g}\frac{\partial^2 A}{\partial y^2} - \frac{\beta}{c_g}|A|^2 A = 0. \tag{3}$$

We seek solutions corresponding to envelopes traveling at an angle $\theta$ to the carrier wave, which can be introduced through the transformation $T \equiv t\cos\theta + y\sin\theta/c_g$, giving from (3),

$$i\left(\frac{\partial A}{\partial x} + \frac{\cos\theta}{c_g}\frac{\partial A}{\partial T}\right) - \frac{\alpha}{c_g^3}(1 - 3\sin^2\theta)\frac{\partial^2 A}{\partial T^2} - \frac{\beta}{c_g}|A|^2 A = 0, \tag{4}$$

i.e., the integrable $1D + 1$ NLSE with a new coefficient in front of the dispersive term, $\alpha' \equiv \alpha(1–3\sin^2\theta)/c_g^3$. At $\theta = \pm\theta_c = \pm\arctan(1/\sqrt{2}) \approx \pm 35.26°$, the dispersive term becomes zero, then switches sign becoming defocusing [26,33]. This is the critical angle examined experimentally herein.

For small-amplitude waves, the nonlinear term in (4) can be neglected, and we have a dispersive linear Schrödinger equation. If $\theta = \pm\theta_c$, the system also becomes nondispersive ($\alpha' = 0$), and the solution can be written as the superposition of two solutions, $A^+ = A(x, T; \theta_c^+)$ and $A^- = A(x, T; \theta_c^-)$ with $\theta_c^+ = +\theta_c$ and $\theta_c^- = -\theta_c$,

$$\begin{aligned} A(x, y, t) = {} & A_0 e^{-\{t\cos\theta_c^+ + \frac{y}{c_g}\sin\theta_c^+ - [(x\cos\theta_c^+)/(c_g)]\}^2/(2\sigma^2)} \\ & + A_0 e^{-\{t\cos\theta_c^- + \frac{y}{c_g}\sin\theta_c^- - [(x\cos\theta_c^-)/(c_g)]\}^2/(2\sigma^2)}, \end{aligned} \tag{5}$$

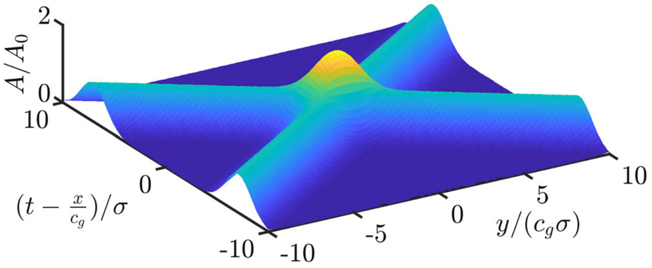

FIG. 1. Theoretical $X$ wave envelope solution formed by two Gaussian envelopes, as parametrized in (5).

where $A_0$ is the theoretical linear focused amplitude of each arm, $\sigma^* \equiv \sigma/\cos(\theta_c)$ is the width of the group in the time domain, and we have chosen Gaussian envelopes. Equation (5) forms the characteristic linear nondispersive $X$-shaped pattern illustrated in Fig. 1. The critical angle also corresponds to the stability boundary of a uniform wave train [33,34]. Single crossed-wave groups traveling at the critical angle are therefore expected to travel without changing shape, as they are both unaffected by GVD and spectral sideband instabilities (see Supplemental Material [35] (SM)]. Because of energy transfer from their highly centralized energy peak, double-crossed wave groups may experience nonstationary behavior, as there are enough components to partake in four-wave interactions [26,36].

*Experimental methodology.—*To examine the effects of crossing at large angles, we carried out experiments in the circular FloWave Ocean Energy Research Facility at The University of Edinburgh (see SM [35], Fig. S3, adapted from [37]). This multidirectional wave basin is encircled by 168 actively absorbing wave makers, enabling creation of waves in all directions. We adopt a Cartesian coordinate system with origin at the center of the tank. The $x$ axis is in the direction of the phase velocity of the carrier waves. Experiments were sufficiently short that reflections did not interfere with incident measurements.

To define a single crossed-wave group, we chose a narrow-banded Gaussian amplitude spectrum in frequency space,

$$\hat{A}(\omega) = \frac{A_0\sigma^*}{\sqrt{2\pi}}\exp\left(-\frac{(\omega - \omega_0)^2\sigma^{*^2}}{2}\right), \tag{6}$$

where $\sigma^*$ is now more generally the group duration, and (6) corresponds to the Fourier transform of a single arm in (5) at $x = y = 0$. The spectral bandwidth ($1/\sigma^*$) was set as large as possible to encourage dispersion at noncritical angles while keeping the group narrow-banded and avoiding distortion of the signal due to the minimum frequency cutoff $\omega_{\min}$ (corresponding to $k_{\min}$; see SM [35]).

Table I summarizes the two types of experiments conducted: single crossed-wave groups (experiment 1a–1d and 2a–2d), consisting of only a positive arm, and $X$ wave groups, consisting of both arms (experiment 3). Both lower-steepness (experiments 1a–1d) and higher-steepness (experiments 2a–2d) single crossed groups were tested, while $X$ wave group experiments were always of a higher steepness. A (nondimensional) spatial nonlinear scale, $\lambda_{\mathcal{N}} = c_g/(\lambda_0\beta|A_0|^2)$ allows the number of wavelengths over which nonlinear effects take place to be estimated.

TABLE I. Experimental parameters, with $\epsilon_{\min}/\epsilon_{\max}$ denoting the minimum/maximum steepness values ($\epsilon \equiv k_0|A|_{\max}$) and $\lambda_{\mathcal{N}}$ the nondimensional nonlinear spatial scale.

| Experiment | $\theta$ (°) | $\omega_0$ (rad s$^{-1}$) | $k_0 d$ | $\sigma^*$ (s) | $\epsilon_{\min}$ | $\epsilon_{\max}$ | $\lambda_{\mathcal{N}}$ |
|---|---|---|---|---|---|---|---|
| 1a | 0 | | | | 0.08 | 0.09 | 24.9 |
| 1b | $\theta_c^+/2$ | | | | 0.08 | 0.09 | 24.9 |
| 1c | $\theta_c^+$ | 7.07 | 10.2 | 2.29 | 0.08 | 0.09 | 24.9 |
| 1d | 40 | | | | 0.08 | 0.08 | 24.9 |
| 2a | 0 | | | | 0.17 | 0.25 | 5.6 |
| 2b | $\theta_c^+/2$ | | | | 0.17 | 0.24 | 5.6 |
| 2c | $\theta_c^+$ | 7.07 | 10.2 | 2.29 | 0.17 | 0.19 | 5.6 |
| 2d | 40 | | | | 0.17 | 0.16 | 5.6 |
| 3 | $\theta_c^+$ and $\theta_c^-$ | 7.07 | 10.2 | 2.29 | 0.18 | 0.26 | 5.0 |

For the single crossed-group experiments, the crossing angle $\theta$ was varied while keeping the group duration $\sigma^*$ constant. Each experiment was repeated four times.

*Results.*—We compare our experimental results with numerical solutions of the $2D+1$ NLSE (split-step Fourier method), using as the boundary condition the complex wave packet amplitude at the first gauge (smallest $x$). We obtain this from the recorded free surface using $A = (\eta + i\tilde{\eta})\exp[-i(k_0 x - \omega_0 t)]$, where $\tilde{\eta}$ is the Hilbert transform of the free surface elevation $\eta$ (e.g., [31]). For single crossed-wave groups, Fig. 2 presents time series of the experimental and numerical packet envelopes (see Fig. S5, SM [35] for spectra). The indicative confidence bands obtained from four repeats of each experiment are not clearly visible due to their proximity to the mean, indicating very good repeatability. We introduce two quantitative measures of dispersion: maximum group amplitude and group duration, which we define through the focus time, $t_f \equiv \sum_{i=1}^N t_i A_i / \sum_{i=1}^N A_i$, in the form of a standard deviation, as

$$t_\sigma \equiv \sqrt{\frac{\sum_{i=1}^N (t_i - t_f)^2 A_i}{\sum_{i=1}^N A_i}}, \tag{7}$$

where the indicator $i$ corresponds to the discrete sampling points in time. Figure 3 shows the change in the maximum amplitude and the group duration from (7) as a function of evolution distances for different crossing angles.

In the lower-steepness case, both experimental and numerical unidirectional packets show clear focusing [Fig. 2(a)] across approximately $10\lambda_0$ of evolution, including a decrease in group duration as the group undergoes dispersive focusing [Fig. 3(b)]. At $\theta = \theta_c^+/2$, the packet shows behavior very similar to unidirectional [Figs. 2(b) and 3(b)], as expected based on linear dispersion [see Fig. S1(b), SM [35] ]. At the critical crossing angle, the amplitude only increases minimally [Fig. 2(c)], and the duration stays constant across the evolution distance [Fig. 3(b)]. Beyond the critical angle, at 40°, changes in the packet amplitude are still within one standard deviation [Fig. 2(d)], and the duration stays constant with minimal changes also predicted by linear theory [see Fig. S1(b), SM [35] ]. For all angles, behavior is well predicted by the $2D+1$ NLSE and predominantly linear, as can be confirmed by the absence of significant spectral changes across the evolution distance [see Figs. S5(a) through S5(d), SM [35] ].

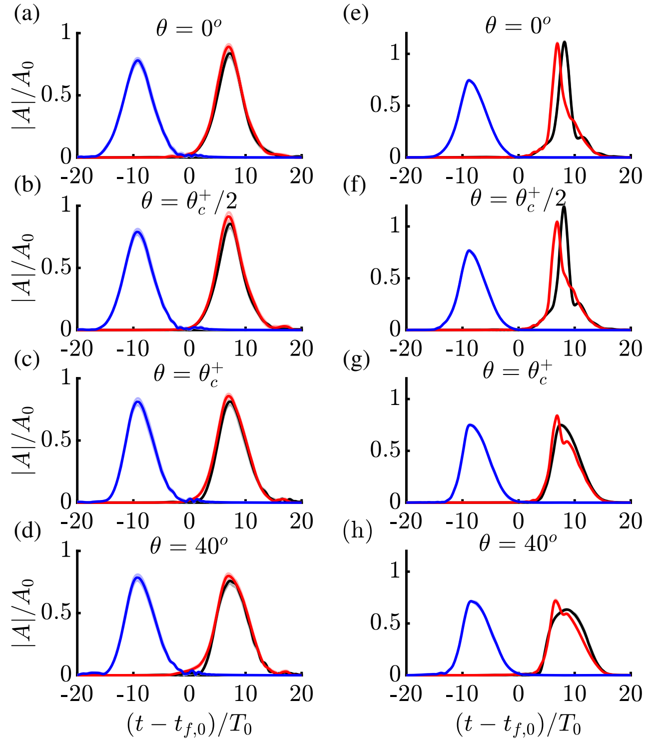

FIG. 2. Envelope time series (normalized by the carrier period, $T_0$) for the single crossed-wave lower-steepness experiments 1a–1d (a)–(d) and the higher-steepness experiments 2a–2d (e)–(h). Blue, red, and black lines denote experiments at the initial ($x/\lambda_0 = -6.67$) gauge, and experiments and numerical solutions at the final ($x/\lambda_0 = 3.60$) gauge, respectively. The dark and light lines show the mean and the confidence bands (± one standard deviation), the latter difficult to distinguish due to strong repeatability.

In the higher-steepness cases, the unidirectional [Fig. 2(e)] and $\theta = \theta_c^+/2$ [Fig. 2(f)] experiments show much more substantial focusing than their lower-steepness counterparts. Nonlinear changes have likely occurred, as is evident from significant spectral changes [Figs. S5(e) and S5(f), SM [35] ], including a drop in peak spectral amplitude and significant spectral widening as a classical signature of modulational instability. The $2D+1$ NLSE (black lines) with its restrictions on steepness and bandwidth captures the main features but not all aspects of the observed behavior for these higher-steepness, close-to-unidirectional cases.

The time-domain behavior of the higher-steepness critical angle experiment [Fig. 2(g)] shows some changes in the packet shape, with larger waves moving to the front of the

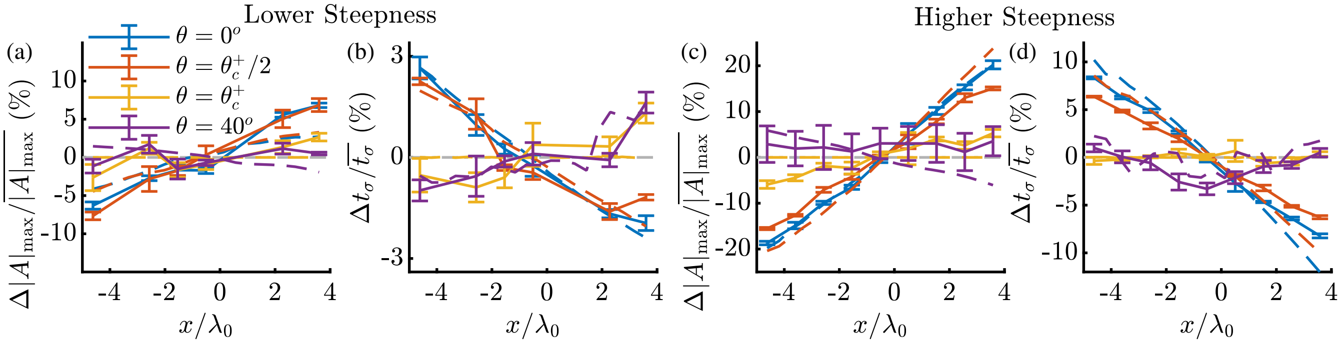

FIG. 3. Relative change of the maximum packet amplitude $\Delta|A|_{\max} = |A|_{\max} - \overline{|A|}_{\max}$ (a),(c) and the group width $\Delta t_\sigma = t_\sigma - \bar{t_\sigma}$ (b),(d) in space for different crossing angles, where $\overline{|A|}_{\max}$ and $\bar{t_\sigma}$ denote averages across the gauges, and $t_\sigma$ is defined by (7). (a),(b) Experiments 1a–1d (lower steepness). (c),(d) Experiments 2a–2d (higher steepness). The continuous and dashed lines denote the mean across repeat experiments with error bars (± one standard deviation) and numerical solutions, respectively.

group creating a double peak, but the maximum amplitude remains largely unchanged [Fig. 3(c)]. The nullification of the dispersive term in the $2D+1$ NLSE at the critical angle has removed linear focusing and stabilized the wave group, as predicted by linear stability analysis [cf. (S2) and Fig. S2 in SM [35] ]. Beyond the critical angle, at 40° [Fig. 2(h)], we observe very similar behavior. The numerical solution of the $2D+1$ NLSE shows these effects clearly with a completely stationary wave group in the group frame for the critical angle [Fig. 2(g)].

Summarizing, it is clear from Figs. 3(c) and 3(d) that, as with the lower-steepness experiments, the behaviors of the 35.26° and the 40° cases are least dispersive, as well predicted by the $2D+1$ NLSE, and that most of the strong nonlinearity observed for small and zero angles is quelled for these larger crossing angles. For the higher-steepness experiments, spectral changes occur that are somewhat greater than predicted by the $2D+1$ NLSE or small but nonzero where zero changes are predicted by the $2D+1$ NLSE [Figs. S5(e) through S5(h), SM [35] ].

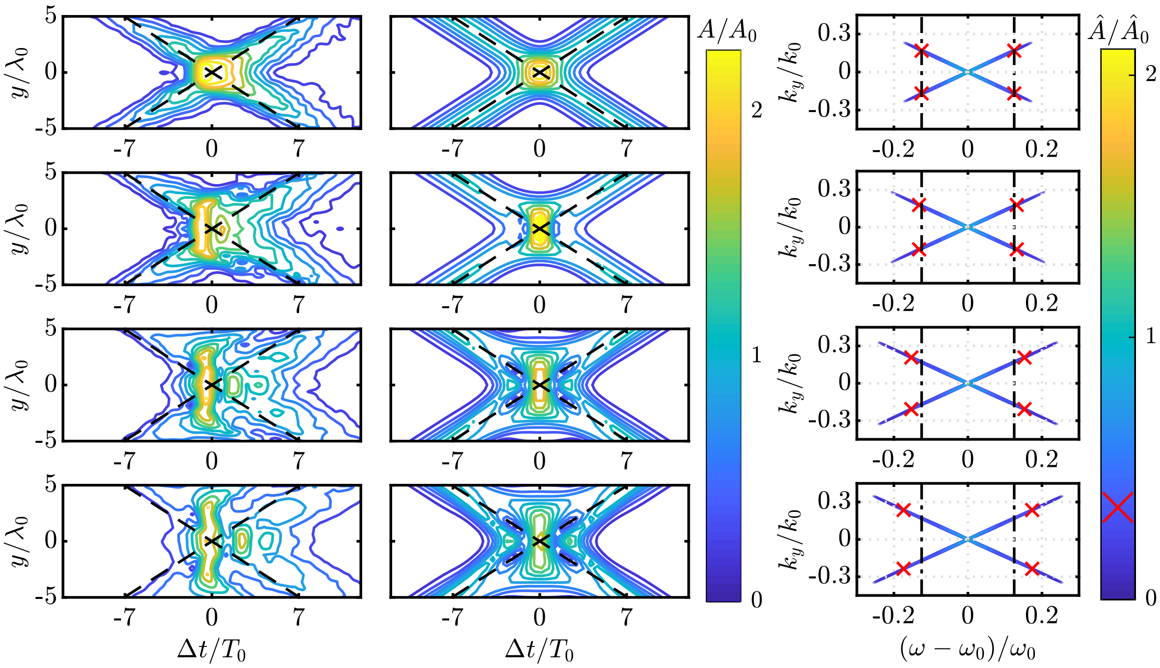

FIG. 4. Spatiotemporal comparison of the experimental (left) and numerical (centre) $X$ wave packet (experiment 3) as the packet evolves in space: $\Delta x/\lambda_0 = -9.6$, $-3.2$, 1.9, 4.4 (rows, descending). The black dashed lines correspond to the 35.26° angle. The amplitude spectra $\hat{A}(\omega, k_y)$ of the numerical results are also presented (right): gray lines are grid lines, red crosses indicate the position of the contour at $\hat{A}/\hat{A}_0 = 0.33$ with the back dash-dotted lines aligned with the crosses in the top panel. We show the spatiotemporal signals in the group reference frame as predicted by linear theory.

Turning from the single-crossed to the double-crossed or $X$ waves (experiment 3), we reconstruct surfaces of measured packet amplitude $A(y,t)$ at different gauge locations and compare with numerical solutions and corresponding spectra $\hat{A}(\omega, k_y)$, as shown in Fig. 4. At the beginning of its evolution (top rows), the experimental $X$ wave structure is clearly visible with distinct arms lying on the $\pm\theta_c$ lines and a centroid of amplitude $2A_0$. The $X$ structure maintains its global shape as it propagates across the tank, although the finite number of straight wave paddles and potential reflections makes perfect generation by constructive superpositioning away from the center and near the boundaries of the tank challenging (cf. large-time behavior in Fig. 4).

For this higher-steepness experiment, the peak at the crossing points of the two arms undergoes considerable narrowing in the $x$ direction (its direction of travel, shown here as time $t$) and broadening in the $y$ direction, a phenomenon previously observed by Gibbs and Taylor for directionally spread groups that are not crossing and described therein as "walls of water" [38]. We observe this behavior in both experiments and numerical simulations of the $2D + 1$ NLSE and note that it arises because of resonant third-order nonlinearity from the interaction between four wave components [36]. Accordingly, the $2D + 1$ NLSE predicts a preferential energy transfer to higher wave numbers, as shown in the right column of Fig. 4. Unlike the single-crossed wave groups, where all the nonzero spectral components are confined to a single line, the double-crossed or $X$ wave has sufficient components to take part in four-wave interaction (cf. Phillips's figure of 8), which for a narrow-banded three-dimensional wave packet has the largest preferential direction of energy transfer to higher-wave numbers at 35.26° [26]. An extended set of numerical solutions for single-crossed groups and $X$ waves confirms that the $2D + 1$ NLSE predicts truly stationary behavior for single-crossed waves at 35.26°; the most long-lived $X$ waves occur at angles close to 35.26° for small steepness, with the angle of maximum lifetime increasing up to approximately 45° for higher steepness (see Figs. S6 and S7, SM [35]).

*Conclusion.*—We have demonstrated experimentally the existence of nondispersive single-crossed wave groups and long-lived nonlinear hydrodynamic $X$ wave packets when a carrier wave is modulated by a wave group crossing it at an angle of approximately ±35.26°, as predicted by the $2D + 1$ NLSE and previously observed experimentally in optics. Our single-crossed wave group experiments showed no linear or nonlinear focusing at the critical angle, with both amplitude and group width remaining constant across the evolution distance regardless of steepness, as predicted by numerical solutions of the $2D + 1$ NLSE.

When the two arms traveling at ±35.26° are superimposed, a nondispersive hydrodynamic $X$ wave is constructed, which we have observed in the laboratory. Such a structure was observed to be quasistationary for a relatively high steepness; however it became subject to third-order resonant four-wave interactions, which are known to transfer energy to higher wave numbers with a preferred direction of ±35.26° [26] and result in the most long-lived $X$ wave structures at angles ±35.26° for small steepness, increasing up to approximately ±45° for higher steepness. In the real ocean, such bimodal seas, with energy traveling in two directions, do not occur infrequently [39], and this preferred growth direction may lead to the natural generation of $X$ waves, which in turn will be long lived due to their lack of dispersion. Although unidirectional groups focused to more extreme amplitudes, the experimental observation of crossed groups propagating unchanged over many wavelengths confirm the lifetime extension of wave groups containing the potential for extreme events.

Finally, this work may motivate new numerical and experimental studies to investigate the applicability of directional coherent structures in different nonlinear dispersive physical media known to be described by the NLSE, where such structures have not yet been observed, such as plasma, Bose-Einstein condensates, and cold gases.

The authors thank E. Nixon, Dr. S. Draycott, and Dr. T. Davey at FloWave. FloWave was funded by the United Kingdom EPSRC (EP/I02932X/1). J. N. S. acknowledges support from an EPSRC studentship (No. 1770088), and T. S. v. d. B. support from a Royal Academy of Engineering Research Fellowship. A. C. acknowledges Takuji Waseda for valuable discussions. M. O. has been funded by Progetto di Ricerca d'Ateneo CSTO160004 and supported by the "Department of Excellence 2018-2022" grant awarded by the Italian Ministry of Education, University and Research (MIUR) (L.232/2016).

[1] C. Conti, S. Trillo, P. Di Trapani, G. Valiulis, A. Piskarskas, O. Jedrkiewicz, and J. Trull, Nonlinear Electromagnetic $x$ Waves, Phys. Rev. Lett. **90**, 170406 (2003).

[2] P. Di Trapani, G. Valiulis, A. Piskarskas, O. Jedrkiewicz, J. Trull, C. Conti, and S. Trillo, Spontaneously Generated $x$-Shaped Light Bullets, Phys. Rev. Lett. **91**, 093904 (2003).

[3] F. Baronio, S. Wabnitz, and Y. Kodama, Optical Kerr Spatiotemporal Dark-Lump Dynamics of Hydrodynamic Origin, Phys. Rev. Lett. **116**, 173901 (2016).

[4] Y. V. Bludov, V. V. Konotop, and N. Akhmediev, Matter rogue waves, Phys. Rev. A **80**, 033610 (2009).

[5] H. Bailung, S. K. Sharma, and Y. Nakamura, Observation of Peregrine Solitons in a Multicomponent Plasma with Negative Ions, Phys. Rev. Lett. **107**, 255005 (2011).

[6] J. N. Brittingham, Focus waves modes in homogeneous Maxwells equations: Transverse electric mode, J. Appl. Phys. **54**, 1179 (1983).

[7] R. W. Ziolkowski, Exact solutions of the wave equation with complex source locations, J. Math. Phys. (N.Y.) **26**, 861 (1985).

[8] R. W. Ziolkowski, Localized transmission of electromagnetic energy, Phys. Rev. A **39**, 2005 (1989).

[9] J. Lu and J. F. Greenleaf, Nondiffracting *X* waves: Exact solutions to free-space scalar wave equation and their finite aperture realizations, IEEE Trans. Ultrason. Ferroelectr. Freq. Control **39**, 19 (1992).

[10] H. A. Willebrand and B. S. Ghuman, Fiber optics without fiber, IEEE Spectrum **38**, 40 (2001).

[11] T. Ito and S. Okazaki, Pushing the limits of lithography, Nature (London) **406**, 1027 (2000).

[12] D. Solli, C. Ropers, P. Koonath, and B. Jalali, Optical rogue waves, Nature (London) **450**, 1054 (2007).

[13] M. J. Ablowitz, *Nonlinear Dispersive Waves: Asymptotic Analysis and Solitons* (Cambridge University Press, Cambridge, England, 2011), Vol. 47.

[14] M. Onorato, S. Residori, U. Bortolozzo, A. Montina, and F. Arecchi, Rogue waves and their generating mechanisms in different physical contexts, Phys. Rep. **528**, 47 (2013).

[15] J. M. Dudley, F. Dias, M. Erkintalo, and G. Genty, Instabilities, breathers and rogue waves in optics, Nat. Photonics **8**, 755 (2014).

[16] F. Baronio, B. Frisquet, S. Chen, G. Millot, S. Wabnitz, and B. Kibler, Observation of a group of dark rogue waves in a telecommunication optical fiber, Phys. Rev. A **97**, 013852 (2018).

[17] A. Chabchoub, B. Kibler, C. Finot, G. Millot, M. Onorato, J. Dudley, and A. Babanin, The nonlinear Schrödinger equation and the propagation of weakly nonlinear waves in optical fibers and on the water surface, Ann. Phys. (Amsterdam) **361**, 490 (2015).

[18] M. Onorato, F. Baronio, M. Conforti, A. Chabchoub, P. Suret, and S. Randoux, Hydrodynamic and optical waves: A common approach for unidimensional propagation, in *Rogue and Shock Waves in Nonlinear Dispersive Media* (Springer, New York, 2016), pp. 1–22.

[19] B. Kibler, A. Chabchoub, A. Gelash, N. Akhmediev, and V. E. Zakharov, Superregular Breathers in Optics and Hydrodynamics: Omnipresent Modulation Instability beyond Simple Periodicity, Phys. Rev. X **5**, 041026 (2015).

[20] R. El Koussaifi, A. Tikan, A. Toffoli, S. Randoux, P. Suret, and M. Onorato, Spontaneous emergence of rogue waves in partially coherent waves: A quantitative experimental comparison between hydrodynamics and optics, Phys. Rev. E **97**, 012208 (2018).

[21] W. H. Hui and J. Hamilton, Exact solutions of a three-dimensional nonlinear Schrödinger equation applied to gravity waves, J. Fluid Mech. **93**, 117 (1979).

[22] M. Onorato, A. R. Osborne, and M. Serio, Modulational Instability in Crossing Sea States: A Possible Mechanism for the Formation of Freak Waves, Phys. Rev. Lett. **96**, 014503 (2006).

[23] A. Toffoli, E. M. Bitner-Gregersen, A. R. Osborne, M. Serio, J. Monbaliu, and M. Onorato, Extreme waves in random crossing seas: Laboratory experiments and numerical simulations, Geophys. Res. Lett. **38**, L06605 (2011).

[24] K. T. O. Gramstad, E. Bitner-Gregersen, and J. N. Borge, Modulational instability and rogue waves in crossing sea states, J. Phys. Oceanogr. **48**, 1317 (2018).

[25] D. H. Peregrine, Water waves, nonlinear Schrödinger equations and their solutions, ANZIAM J. **25**, 16 (1983).

[26] M. S. Longuet-Higgins, On the nonlinear transfer of energy in the peak of a gravity-wave spectrum: A simplified model, Proc. R. Soc. A **347**, 311 (1976).

[27] V. P. Ruban, Enhanced rise of rogue waves in slant wave groups, JETP Lett. **94**, 177 (2011).

[28] V. P. Ruban, Breathing rogue wave observed in numerical experiment, Phys. Rev. E **74**, 036305 (2006).

[29] V. Ruban, Nonlinear Stage of the Benjamin-Feir Instability: Three-Dimensional Coherent Structures and Rogue Waves, Phys. Rev. Lett. **99**, 044502 (2007).

[30] V. E. Zakharov, Stability of periodic waves of finite amplitude on the surface of a deep fluid, J. Appl. Mech. **9**, 190 (1968).

[31] A. Osborne, *Nonlinear Ocean Waves and the Inverse Scattering Transform* (Academic Press, New York, 2010).

[32] A. Chabchoub and R. Grimshaw, The hydrodynamic nonlinear Schrödinger equation: Space and time, Fluids **1**, 23 (2016).

[33] P. G. Saffman and H. C. Yuen, Stability of a plane soliton to infinitesimal two-dimensional perturbations, Phys. Fluids **21**, 1450 (1978).

[34] H. C. Yuen and B. M. Lake, *Nonlinear Dynamics of Deep-Water Gravity Waves* (Elsevier, New York, 1982), pp. 67–229.

[35] See Supplemental Material at http://link.aps.org/supplemental/10.1103/PhysRevLett.123.184501, which includes Refs. [33,34], for a discussion of linear dispersion and stability and of the experimental methodology, free surface time series, and extended numerical simulations.

[36] O. Phillips, On the dynamics of unsteady gravity waves of finite amplitude part 1. The elementary interactions, J. Fluid Mech. **9**, 193 (1960).

[37] D. R. Noble, Engineering Doctorate Thesis, University of Edinburgh, 2017.

[38] R. Gibbs and P. Taylor, Formation of walls of water in “fully” nonlinear simulations, Applied Ocean Research **27**, 142 (2005).

[39] K. Ewans, Observations of the directional spectrum of fetch-limited waves, J. Phys. Oceanogr. **28**, 495 (1998).